

# Non-Reciprocal Transmission and Reflection of a Chirally-Coupled Quantum Dot

D.M. Price,<sup>1,\*</sup> D.L. Hurst,<sup>1,\*</sup> C. Bentham,<sup>1</sup> M.N. Makhonin,<sup>1</sup> B. Royall,<sup>1</sup>  
E. Clarke,<sup>2</sup> P. Kok,<sup>1</sup> L.R. Wilson,<sup>1</sup> M.S. Skolnick,<sup>1</sup> and A.M. Fox<sup>1,†</sup>

<sup>1</sup>*Department of Physics and Astronomy, University of Sheffield,  
Hounsfield Road, Sheffield, S3 7RH, United Kingdom*

<sup>2</sup>*EPSRC National Epitaxy Facility, Department of Electronic and Electrical Engineering,  
University of Sheffield, Sheffield S1 3JD, United Kingdom*

(Dated: January 31, 2018)

We report non-reciprocal transmission and reflection for quantum dot exciton spins coupled to nano-photonic waveguides. A clear dependence on propagation direction is found for a chirally-coupled quantum dot, with spin up and spin down exciton spins coupling to the left and right propagation directions respectively. The reflection signal shows an opposite trend to the transmission, which a numerical model indicates is due to direction-selective saturation of the dot. The chiral spin-photon interface we demonstrate breaks reciprocity of the system, and opens the way to spin-based quantum optical components such as optical diodes and circulators in a chip-based solid-state environment.

## I. INTRODUCTION

The deterministic coupling of a two-level system (TLS) to a one-dimensional waveguide has been shown to provide a near-ideal platform for demonstrating quantum-optical effects such as single-photon nonlinearities [1]. A key parameter for such “1-D atoms” is the  $\beta$ -factor, which quantifies the relative coupling to the waveguide compared to other optical modes. In the limit of  $\beta \rightarrow 1$ , and in the coherent limit, the scattering of a single photon from the TLS results in its complete reflection with an associated  $\pi$  phase shift [2]. By contrast, when the incident state is composed of two photons, the potential for the formation of a bound state causes preferential transmission of the wave-packet [3], leading to bunched statistics in the transmitted field and the formation of an efficient single-photon nonlinearity. In the case where  $\beta$  is smaller than unity, and/or dephasing is present, the same effects occur but with smaller magnitude. Such effects have been observed in a variety of systems, notably semiconductor quantum dots (QDs) coupled to photonic crystal waveguides [4, 5] and SiV or GeV centres coupled to nanobeams [6–8], with transmission dips as low as 60% now reported [9].

The recent discovery of non-reciprocal coupling between dipole emitters and nano-photonic structures [10–17] adds a completely new dimension to the system. These chiral effects arise from the spin-orbit interaction of light [18], and lead to directionality in the  $\beta$ -factor, with circular dipoles of opposite sense coupling to modes propagating in opposite directions. The result of a transmission-type experiment on a chirally-coupled emitter has to be different to the non-chiral case, as the emitter does not couple to the backward propagating mode and hence reflection is not possible. In the coherent, single-photon limit, light is now transmitted with 100%

probability but accumulates a  $\pi$  phase shift, previously reserved for the reflected component. This forms the basis for a spin-dependent phase-shift, which can be used to implement a scalable quantum network [19].

The ideal behaviour is hard to observe in practice: the  $\beta$ -factor is never perfect and dephasing is always present to some extent. Moreover, the directional coupling efficiency is less than unity. In these non-ideal conditions, the behaviour is expected to lie somewhere between the limits of perfect reflection and perfect transmission for the non-chiral and chiral cases respectively. In this paper, we present experimental data on a single QD chirally coupled to a nanobeam waveguide and then use a theoretical model to describe the system. The key finding is the observation of a spin-dependent dip in the transmission, which is strongly directionally dependent and breaks reciprocity. We also present experimental data on spin-dependent reflectivity, where unexpectedly, the more weakly coupled dipole gives the larger signal. The theoretical modelling shows that this counter-intuitive behaviour is caused by partial saturation of the more strongly coupled QD spin at the power levels used in the experiment.

## II. THE SYSTEM

Figure 1 shows schematically the system under consideration. A QD is coupled to the single optical mode of a nanobeam waveguide and driven by a resonant laser field. The laser scatters from the QD and is either transmitted through the waveguide, reflected back in the direction of the laser input or lost from the sample, as shown in Fig. 1a. The non-chiral interaction of a dot with a resonant laser field has been studied in Refs. [4, 5, 9]. In this paper we are interested in a dot located at a circular polarization point (C-point) [14, 20] of the waveguide, where the QD exciton spin couples to the direction of propagation [16, 21].

The non-reciprocal spin-photon coupling of a chirally-

\* These authors contributed equally to the project.

† [mark.fox@sheffield.ac.uk](mailto:mark.fox@sheffield.ac.uk)

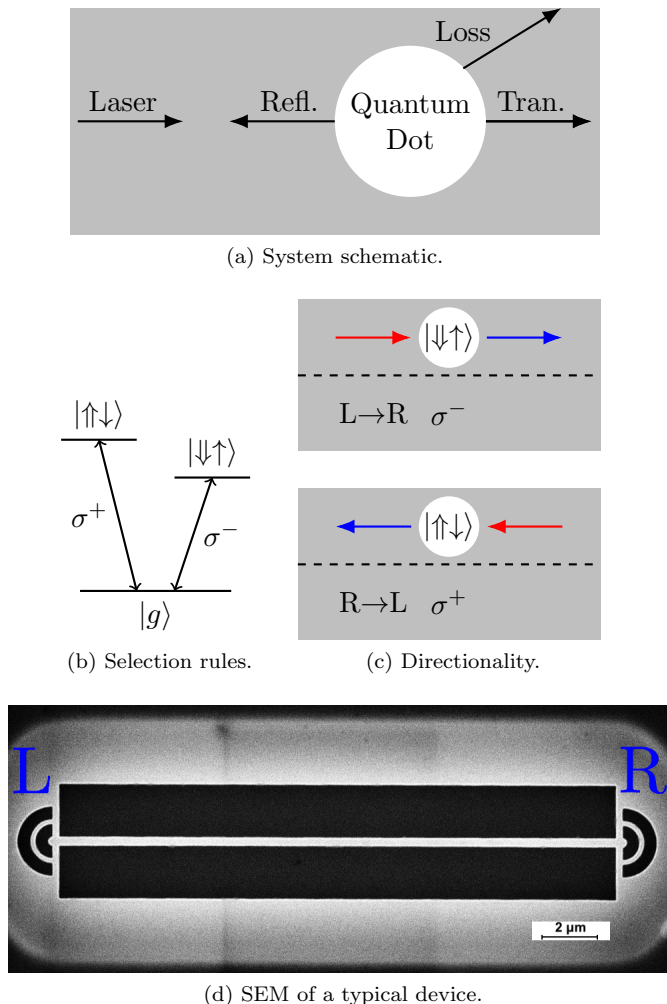


FIG. 1. Schematic of the system. Fig. 1a shows a laser coupled into a section of waveguide containing a QD, which is located at a C-point. The laser is either transmitted down the waveguide, reflected from the QD back down the waveguide or scattered into a continuum of free-space loss modes. Fig. 1b shows selection rules for exciton transitions. The  $\{\uparrow, \downarrow\}$  and  $\{\downarrow, \uparrow\}$  symbols refer to holes and electrons, respectively. The splitting of the transitions is caused by a Faraday-geometry magnetic field. Fig. 1c illustrates the directional spin-photon coupling. Emission and resonant scattering are shown by the blue and red arrows respectively. The exciton spin states that are coupled to the mode are indicated with the same notation as in 1b. Fig. 1d shows a scanning electron microscope (SEM) image of a typical nanobeam waveguide with the left (L) and right (R) out-couplers labelled.

coupled QD (i.e. a QD at a C-point) arises from two factors: the chiral properties of the waveguide modes, and the strict selection rules for QD exciton transitions. The chirality of the modes originates from the strong light confinement in the nanobeam, which has lateral dimensions comparable to the wavelength. The longitudinal and transverse electromagnetic field components have a  $\pm\pi/2$  phase difference between them, with the sign depending on the direction of propagation. At C-points,

the magnitudes are equal, and we thus have circularly polarised modes with rotation sense depending on the direction. The waveguide itself is inherently non-chiral and the chirality arises from the breaking of the symmetry at off-centre locations.

The QD selection rules are illustrated in Fig. 1b. Spin up ( $|\uparrow\downarrow\rangle$ ) or down ( $|\downarrow\uparrow\rangle$ ) excitons couple respectively to  $\sigma^+$  or  $\sigma^-$  circularly polarised light in order to preserve angular momentum. When such a QD is positioned at a C-point, the opposite circular polarizations propagate in different directions. The selection rules then imply that opposite spin excitons couple to modes propagating in opposite directions. This applies both to emission, as shown schematically by the blue arrows in Fig. 1c, and to resonant scattering of incoming photons, as represented by the red arrows.

As mentioned in the introduction, the transmission of an ideal system is 100% for both QD spin states, but with a  $\pi$  phase shift for the transition that couples to the mode. The behaviour of a realistic system is more complicated, being highly sensitive to a number of key parameters.

**The directional coupling factor:** This gives the probability that an exciton with given spin will emit preferentially to the left (L) or right (R), and is described by four parameters:  $\zeta_L^+$ ,  $\zeta_R^+$ ,  $\zeta_L^-$  and  $\zeta_R^-$ , where + and - represent the dipole spin. For ideal chiral-coupling, we would have  $\zeta_L^+ = \zeta_R^- = 1$ , and  $\zeta_L^- = \zeta_R^+ = 0$ . However, experimental values might be  $\zeta_L^+ = \zeta_R^- = 0.95$  and  $\zeta_L^- = \zeta_R^+ = 0.05$ , owing to positioning of the QD slightly away from an ideal C-point.

**The overall  $\beta$ -factor:** The modelling of an ideal point-like circular dipole emitter at a C-point of a nanobeam waveguide indicates that the total coupling corresponds to a best overall  $\beta$ -factor of around 70% [16]. This means that an excited QD will, with 30% probability, emit a photon into an unguided optical mode.

**The pure dephasing rate:** The characteristic features in the transmission and reflection spectra rely on interference between the incident and scattered optical fields, making them highly sensitive to decoherence, which is described by the pure-dephasing time  $\tau_d$  [22].

**Spectral wandering and blinking:** The charge environment around the QD is unstable and this causes line broadening as the exciton energy wanders on timescales set by charging and discharging of nearby trap states. Furthermore, there is always some finite probability  $P_{\text{dark}}$  that a photon arriving at the QD will find it in some optically inactive or ‘dark’ state. Both of these effects reduce the visibility of the resonant features in the spectra.

Let us consider an imperfect dipole emitter located close to a C-point in a nanobeam waveguide, as illustrated in Fig. 1c. We assume that the dot has 95% directionality, with a left-to-right (L→R) beam coupling predominantly to the  $|\downarrow\uparrow\rangle$  dipole, and vice versa for right-to-left (R→L). The overall  $\beta$  factor is taken to be 70%, and we assume that the response of the QD is partially incoherent due to pure dephasing. A laser beam propagating from L→R will drive the QD strongly when resonant with the  $|\downarrow\uparrow\rangle$  dipole. This will cause both interference between scattered and incident fields, as well as emission into environmental loss modes, causing a dip in the transmission. A much smaller dip is expected when resonant with the  $|\uparrow\downarrow\rangle$  dipole, as it couples only very weakly to the laser. We thus expect to see a strong difference in the transmission for the opposite circular dipoles, in agreement with the experimental data of Sec. III. The theoretical modelling in Sec. IV further reproduces this effect and clarifies that the depth of the  $|\downarrow\uparrow\rangle$  dip in our sample is limited by a combination of dephasing, spectral wandering and blinking.

We can intuitively argue that the behaviour expected in a reflection geometry is significantly different. Consider a L→R input laser, coupling with relative efficiency of  $\sim 95\%$  to the  $|\downarrow\uparrow\rangle$  dipole, which is in turn coupled with  $\sim 5\%$  efficiency to the R→L mode. By contrast, the  $|\uparrow\downarrow\rangle$  dipole couples with relative efficiency of 5% to the L→R mode but 95% efficiency to the R→L mode. As a first-order approximation then, ignoring the interference effects that dominate in symmetrically-coupled systems, we might expect to see the *same* reflected signal from both components. The fraction of the laser coupled into the R→L mode is  $\sim (95\% \times 5\%)^2 \approx 0.2\%$  in both cases (note that the reflected and transmitted intensities are dependent on the *square* of the  $\beta$ -factor [9]). This intuitive result is reproduced by our numerical model provided the power input to the system remains low. On increasing the incident laser power towards the saturation limit of the QD, a qualitatively different behaviour is observed in experiment, with the reflection of a L→R beam being much stronger for the  $|\uparrow\downarrow\rangle$  dipole. This asymmetry is reproduced by our numerical model, and can also be intuitively understood: the transition that couples strongly to the incoming laser saturates first, leading to relatively stronger reflection for the *other*, nominally forbidden, transition.

### III. EXPERIMENTAL RESULTS

The experiments were carried out on single QDs embedded in vacuum-clad single-mode waveguides. The InGaAs quantum dots were grown by the Stranski-Krastanov technique and were embedded in 140 nm thick GaAs regions, grown on top of a 1  $\mu\text{m}$  thick AlGaAs sacrificial layer. Nanobeam waveguides of thickness 280 nm and height 140 nm were produced by a combination of electron-beam-lithography and wet and dry etching.

Second-order Bragg-grating in/out-couplers [23, 24] were added on both ends of the waveguides for coupling to external laser fields. A scanning electron microscope image of a typical structure is shown in Fig. 1d. Further details of the sample structure and fabrication may be found in Ref. [25].

The measurements were made at 4 K in a confocal system with separate control of excitation and detection spots. The spatial resolution was 1–2  $\mu\text{m}$  [26], and a Faraday-geometry magnetic field  $B$  was applied to split the  $\sigma^+$  and  $\sigma^-$  Zeeman transitions. This provides a convenient method to observe the interactions of a resonant laser field with well-defined spin states of the QDs.

Quantum dots near C-points were identified by non-resonantly excited photoluminescence (PL), indicated schematically by the blue arrows in Fig. 1c. 808 nm laser was focussed from above the waveguide and PL was collected from the left and right out-couplers. Over 50 randomly positioned dots were examined to find ones with highest spin-dependent directionality. We define the contrast ratio  $C_L$  as

$$C_L \equiv \zeta_L^+ - \zeta_L^-, \quad (1)$$

which can be determined by measuring the difference in respective intensities of the  $\sigma^+$  and  $\sigma^-$  Zeeman components collected from the left outcoupler. The contrast ratio  $C_R$  is defined equivalently. A contrast ratio of zero would correspond to a symmetrically left/right coupled QD and  $\pm 1$  to a perfectly chirally-coupled QD. The PL spectra at  $B = 1$  T for the QD employed in most of this work are shown in Fig. 2. Values of  $C_R = -0.91$  and  $C_L = 0.84$  are found, with  $\sigma^+$  light propagating predominantly to the left and  $\sigma^-$  predominantly to the right, as in Fig. 1c. The large degree of directionality shows the strongly chiral coupling for this particular QD.

Having identified a chirally-coupled QD, we now investigate the non-reciprocal behaviour in resonant transmission. The geometry for the experiment is shown schematically in Fig. 1c. A tunable single-frequency laser is incident on one of the out-couplers and the transmitted light detected from the opposite out-coupler. An 808 nm non-resonant repump laser was applied to stabilise the QD charge state [25]; no resonant transmission dips were observed without the repump laser. The QD charge state is not known with certainty, but this is not important as both charged and neutral excitons emit circularly-polarised light that couples to the chiral fields [16]. In fact, it is most likely that we have a charged exciton, since the repump laser creates free electron-hole pairs.

The repump laser beam was mechanically chopped at 500 Hz, and lock-in techniques employed to maximise the signal to noise in the detection of the resonant laser transmitted to the output-coupler [27]. We obtain transmission spectra by dividing the detected intensity with the repump laser on to that without it, where there is no interaction with the QD. A magnetic field of 1 T was employed for the resonant transmission experiments, sufficient to give well-resolved Zeeman components within

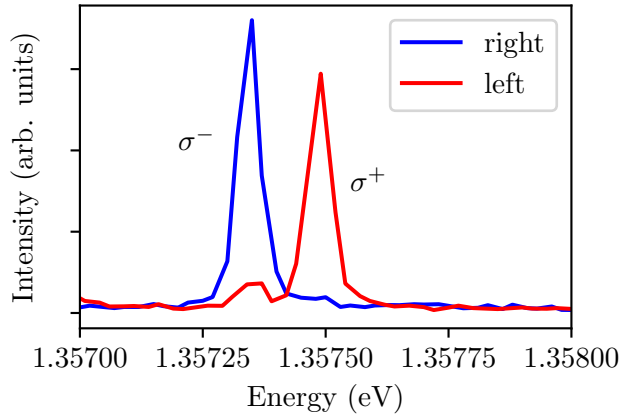


FIG. 2. PL Spectra for the Zeeman components of the chirally coupled QD at  $B = 1$  T, collected from the left and right outcouplers (see Fig. 1c). The observed linewidths are resolution limited and also likely increased by the employed non-resonant excitation.

the mode-hop-free scan range of the laser.

Resonant transmission spectra for L→R propagation are shown in Fig. 3a, and for the reverse case of R→L propagation in Fig. 3b. Energies are measured as a function of detuning from the exciton transition energy at  $B = 0$ . Clear signals from both the  $\sigma^-$  and  $\sigma^+$  exciton transitions are seen. The asymmetric, Fano-resonance lineshapes are due to interference between the laser scattered by the QD and the spectral quasi-continuum arising from Fabry-Perot modes of the nanobeam which form due to back-scattering from the in and out-couplers [4]. In Fig. 3a for L→R propagation, the  $\sigma^-$  dip is dominant, with the  $\sigma^+$  dip  $\sim 10$  times weaker. Complementary behaviour is observed for R→L propagation in Fig. 3b:  $\sigma^+$  is the dominant transition,  $\sim 2.5$  times stronger than  $\sigma^-$ . Contrast ratios in transmission between the  $\sigma^-$  and  $\sigma^+$  components for propagation from L→R (R→L) are found to be  $-0.79$  ( $0.45$ ), indicating a strong left/right asymmetry between the coupling rates, with the dominant component switching upon changing propagation direction. This strong non-reciprocity in the transmission data is in agreement with the theoretical results shown in Fig. 5a and the intuitive discussion of Sec. II.

Figures 4a and 4b present results obtained in the reflection geometry. In Fig. 4a, the resonant laser is incident from the left grating-coupler and detected in back-scattering from the same grating. In marked contrast to the transmission experiment of Fig. 3a, a stronger peak is seen for  $\sigma^+$ , with only a weak feature at  $\sigma^-$ . The opposite is observed when the laser is incident from the right coupler, as shown in Fig. 4b.

The predominance of the reflection signal from the spin that couples only weakly to the incoming mode is, at first, rather surprising: one might naively expect that the QD

transition coupled most strongly to the mode would show the strongest reflection. This would certainly be true for a non-chiral QD, but it is not the expected behaviour for a chirally-coupled QD. As explained in Sec. II, the reflected signals are expected to have equal strengths at low powers and then the less well coupled transition is expected to dominate at higher powers. The low-power regime is characterised by the balancing of the stronger coupling to the laser with weak back-scatter coupling, and vice versa, while the high-power regime has the strongly coupled transition saturating. In our experiments it was not possible to collect reflection data in the low power regime, due to the impractical integration times that would be required, and the results presented in Figs 4a and 4b were acquired when partial saturation of the QD was occurring, as discussed in the next section. The observed results are thus, in fact, exactly what should be expected: this behaviour is reproduced in the theoretical model presented in Sec. IV.

Finally, we conclude by mentioning the control experiment described in the Supplemental Material. There we show the results for a non-chiral system, where the QD is positioned close to the centre of the waveguide. It is evident that the non-reciprocal response of the chirally-coupled QD in transmission and reflection is not present when chiral-coupling is removed from the system.

#### IV. MODELLING

We now present numerical modelling of the system shown in Fig. 1. In the supplemental material we show how the Input-Output formalism [28] can be used to derive explicit expressions for the left and right optical field amplitudes with an input laser driving the system from the left. It is then necessary, in order to account for spectral wandering and blinking of the QD, to convolve the transmission spectrum implied by these amplitudes with a Gaussian function describing the distribution of exciton energies actually being probed. This is characterised by the parameter  $\sigma$ —the variance of the distribution.

The numerical results that are obtained depend strongly on several key sample parameters, especially the radiative lifetime  $\tau$  of the QD, the pure dephasing time  $\tau_d$  and the variance of the Gaussian noise profile  $\sigma$ . The value of  $\tau$  can be directly measured and is found to be  $0.95$  ns for this QD. The spectral wandering profile and pure dephasing rates of the QD are more challenging to extract directly, although a lower limit of  $\tau_d > 120$  ps is set by the  $8$   $\mu$ eV linewidth. Given the spectral wandering the actual value of  $\tau_d$  is expected to be longer than this. In the following we use  $\tau = 1$  ns,  $\tau_d = 800$  ps and  $\sigma = 4$   $\mu$ eV, reasonable semi-quantitative estimates [4, 5, 13].

Other key parameters are the overall  $\beta$ -factor of the QD-waveguide system and the directional coupling factor  $\beta_d$ , which we define as the fraction of emission by the QD into the waveguide that propagates to the right. As



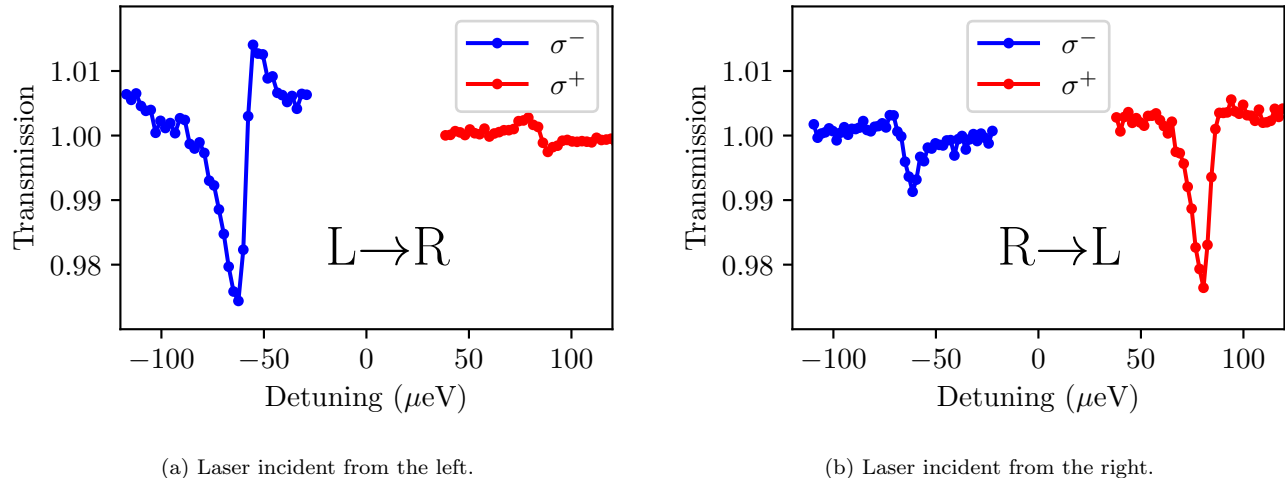


FIG. 3. Waveguide transmission spectra for incident L→R and R→L laser at  $B = 1$  T. Points are normalised to a spectrum obtained without the re-pump laser, i.e. with the QD ‘switched off.’ For light propagating to the right (left) a 3% resonant dip for the  $\sigma^-$  ( $\sigma^+$ ) component is observed and a much weaker dip of  $\sim 0.3\%$  for the  $\sigma^+$  ( $\sigma^-$ ) component. Contrast ratios between the magnitudes of the  $\sigma^-$  and  $\sigma^+$  features of -0.79 and 0.45 for the left and right propagation directions respectively are found.

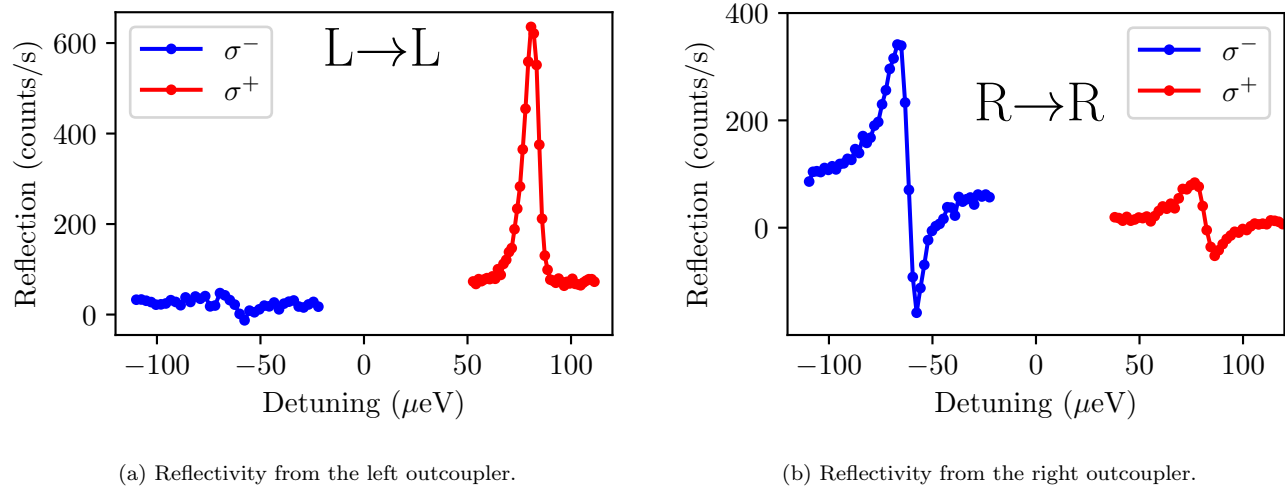


FIG. 4. Reflectivity spectra from the left and right sides of the waveguide at  $B = 1$  T. The peaks that are dominant in reflection are opposite to those in transmission. Light was not simultaneously collected from both out-couplers and hence normalisation of the reflectivity spectra is not possible. The spectra were however collected at the *same* incident power and so comparison between peak magnitudes within Figs. 4a and 4b is meaningful.

discussed in Sec. II, we take  $\beta_d = 0.95$  and  $\beta = 0.7$ . The central energy of the QD is set at 1.3 eV, and the splitting between low and high energy Zeeman components is 0.16 meV, with the lower frequency component having the stronger coupling. Finally, we note that the magnitude of the features we observe depends on the quantity  $P_{\text{dark}}$ , describing the probability that at a given time the QD is in some optically inactive dark state. There is no direct method by which we can extract a value of  $P_{\text{dark}}$  given the obtained data but previously reported values (e.g. in Refs. [4, 5]) fall within the range  $0 \leq P_{\text{dark}} \leq 0.5$

and so  $P_{\text{dark}} = 0.25$  forms a reasonable estimate.

The calculated transmission spectra are shown in Fig. 5a. The results agree with the intuition discussed in Sec. II and qualitatively with the experimental data of Sec. III. The transmission dips are asymmetric, with the dip being stronger for the component preferentially coupled to the QD and less visible for the high energy component. We furthermore note that the size of this dip is strongly dependent on the input power, which indicates that the system is saturated at incident powers of the order of 1 nW. Note however that this refers to

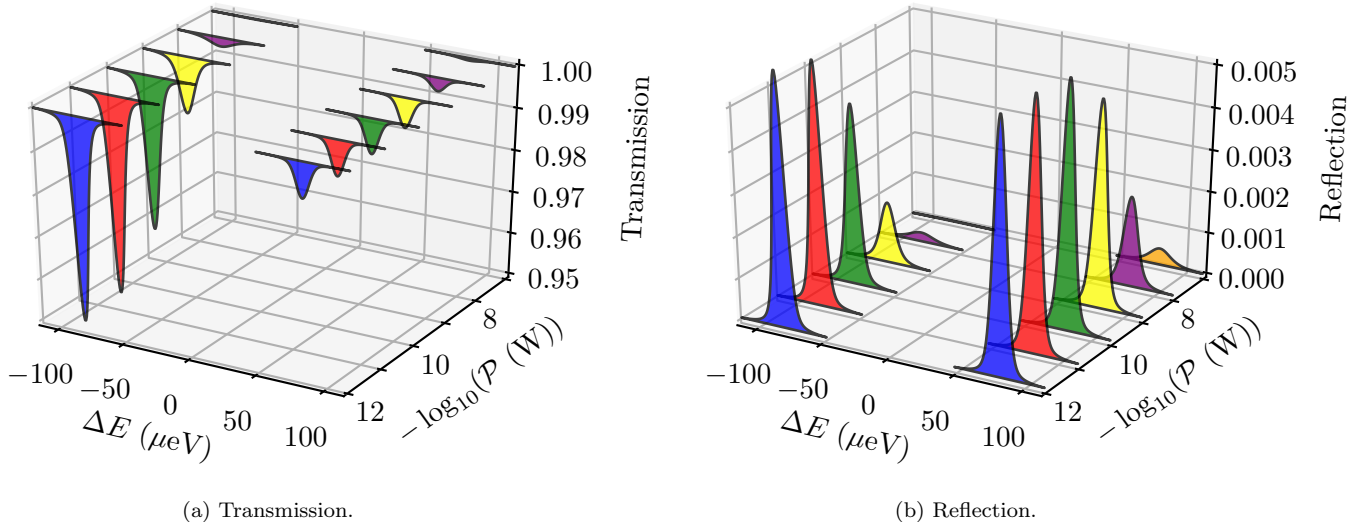


FIG. 5. Calculated transmission and reflection of the system for incident L→R laser driving. Lifetime of the QD is taken as  $\tau = 1$  ns with a pure-dephasing time of  $\tau_d = 800$  ps. We assume imperfect chiral-coupling and therefore  $\beta_d = 0.95$  and  $\beta = 0.7$ . Both spectra are normalised to the incoming laser intensity and calculated with spectral variance  $\sigma = 4$   $\mu\text{eV}$  and dark state probability  $P_d = 0.25$ . Powers of 1, 10 and 100 pW are represented by blue, red and green curves respectively, with 1, 10 and 100 nW shown in yellow, purple and orange.

the power impinging on the QD and is related to, but not directly given by, the laser power incident upon the sample in experiment.

The calculated reflectivity spectra are plotted in Fig. 5b. The spectra at low powers show the reflectivity peaks for each spin component to be of equal height—as discussed qualitatively in Sec. II. However asymmetry develops at higher powers, with the less well coupled transition at higher frequency dominating. This agrees with the experimental results in Figs. 4a and 4b and indicates that the asymmetry is indeed caused by saturation.

In order to obtain a more thorough comparison of experiment and theory, we need to relate the power levels used in the model to those for the measured spectra. The powers used numerically are those *within* the waveguide—after unknown coupling losses—and this makes direct comparison difficult. We can however make a useful relative calibration by plotting the power dependence of the stronger transmission dip. In Fig. 6, we plot power saturation curves for both the model and experiment. By comparing the forms of the experimental and theoretical curves, it is apparent that the input power used for the experiments (50 nW) is equivalent to a few hundred pW in the simulation. Here the ratio between transmission dips is between 4 : 1, for 1 nW and 7 : 1 for 100 pW—see Fig. 5a. This is in semi-quantitative agreement with the experimental results of Fig. 3a, which show a ratio of  $\sim 10 : 1$ .

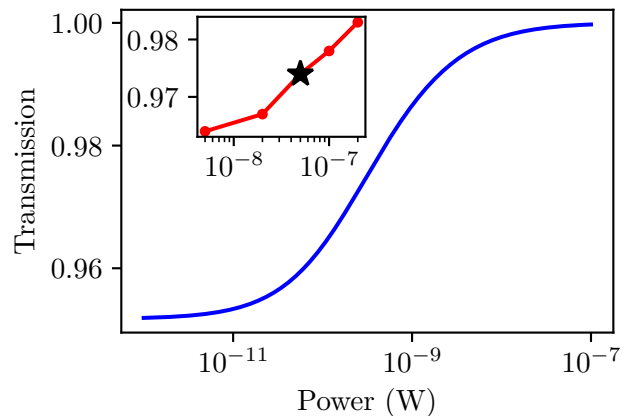


FIG. 6. Theoretical power dependence of the system's transmission dip on resonance for the preferentially coupled component. Inset is the experimentally measured dependence. The power employed for resonant transmission and reflection experiments is indicated by the black star marker. The weakness of the less-well coupled component precluded the study of its variation with power.

## V. CONCLUSIONS

We have reported non-reciprocal transmission for a QD chirally coupled to the electromagnetic field supported by a nano-photonics waveguide. The key experimental result

is the observation of a spin-dependent dip in the transmission spectrum, varying with the direction of propagation. This finding is in agreement with both intuitive arguments and our theoretical model of the system. The results observed in reflection geometry are initially counter-intuitive, with the more weakly-coupled transition giving a larger signal. We have shown that this is caused by partial saturation of the more-strongly coupled transition. Further work with narrower-linewidth dots in charge-stabilised structures [5, 9] and with Purcell enhancement [5, 29], is expected to lead to the observation of deeper transmission dips so that the power dependence of the reflectivity can be explored in more detail. This would also take us closer to the regime where a single photon can be deterministically imparted with a  $\pi$ -phase shift on transmission.

The proof-of-principle results demonstrated in the paper have the potential to pave the way towards a spin-photon interface that would have applications in communication and quantum information technologies [30]. For example, this could open the way to the realisation of on-chip, compact optical diodes operating at the single-photon level [31], single-photon logic devices where the spin state is switched by external laser control [14], and spin-based quantum networks [19], where quantum information is transmitted by emitted photons in a scalable, on-chip geometry.

## ACKNOWLEDGMENTS

This work was funded by the EPSRC (UK) Programme Grants EP/J007544/1 and EP/N031776/1.

- 
- [1] Darrick E. Chang, Vladan Vuletić, and Mikhail D. Lukin, “Quantum nonlinear optics —photon by photon,” *Nature Photonics* **8**, 685 (2014).
- [2] S. Fan, S. E. Kocabas, and J. T. Shen, “Input-output formalism for few-photon transport in one-dimensional nanophotonic waveguides coupled to a qubit,” *Phys. Rev. A* **82**, 063821 (2010).
- [3] Huaixiu Zheng, Daniel J. Gauthier, and Harold U. Baranger, “Waveguide qed: Many-body bound-state effects in coherent and fock-state scattering from a two-level system,” *Phys. Rev. A* **82**, 063816 (2010).
- [4] A. Javadi, I. Söllner, M. Arcari, S. Lindskov Hansen, L. Midolo, S. Mahmoodian, G Kiršanskė, T. Pregnolato, E. H. Lee, J. D. Song, S. Stobbe, and P. Lodahl, “Single-photon non-linear optics with a quantum dot in a waveguide,” *Nature Communications* **6**, 8655 (2015).
- [5] D. Hallett, A. P. Foster, D. L. Hurst, B. Royall, P. Kok, E. Clarke, I. E. Itskevich, A. M. Fox, M. S. Skolnick, and L. R. Wilson, “Electrical control of nonlinear quantum optics in a nano-photonic waveguide,” ArXiv e-prints (2017), [arXiv:1711.00682 \[quant-ph\]](https://arxiv.org/abs/1711.00682).
- [6] A. Sipahigil, R. E. Evans, D. D. Sukachev, M. J. Burek, J. Borregaard, M. K. Bhaskar, C. T. Nguyen, J. L. Pacheco, H. A. Atikian, C. Meuwly, R. M. Camacho, F. Jelezko, E. Bielejec, H. Park, M. Lončar, and M. D. Lukin, “An integrated diamond nanophotonics platform for quantum-optical networks,” *Science* **354**, 847–850 (2016).
- [7] M. K. Bhaskar, D. D. Sukachev, A. Sipahigil, R. E. Evans, M. J. Burek, C. T. Nguyen, L. J. Rogers, P. Siyushev, M. H. Metsch, H. Park, F. Jelezko, M. Lončar, and M. D. Lukin, “Quantum nonlinear optics with a germanium-vacancy color center in a nanoscale diamond waveguide,” *Phys. Rev. Lett.* **118**, 223603 (2017).
- [8] Michael J. Burek, Charles Meuwly, Ruffin E. Evans, Mihir K. Bhaskar, Alp Sipahigil, Srujan Meesala, Bartholomeus Machielse, Denis D. Sukachev, Christian T. Nguyen, Jose L. Pacheco, Edward Bielejec, Mikhail D. Lukin, and Marko Lončar, “Fiber-coupled diamond quantum nanophotonic interface,” *Phys. Rev. Applied* **8**, 024026 (2017).
- [9] Henri Thyrrestrup, Gabija Kiršanskė, Hanna Le Jeannic, Tommaso Pregnolato, Liang Zhai, Leonardo Midolo, Nir Rotenberg, Alisa Javadi, Rüdiger Schott, Andreas D. Wieck, Arne Ludwig, Matthias C. Löbl, Immo Söllner, Richard J. Warburton, and Peter Lodahl, “Quantum optics with near lifetime-limited quantum-dot transitions in a nanophotonic waveguide,” arXiv:1711.10423 (2017).
- [10] Christian Junge, Danny O’Shea, Jürgen Volz, and Arno Rauschenbeutel, “Strong coupling between single atoms and nontransversal photons,” *Phys. Rev. Lett.* **110**, 213604 (2013).
- [11] Jan Petersen, Jürgen Volz, and Arno Rauschenbeutel, “Chiral nanophotonic waveguide interface based on spin-orbit interaction of light,” *Science* **346**, 67–71 (2014).
- [12] Francisco J. Rodríguez-Fortuño, Isaac Barber-Sanz, Daniel Puerto, Amadeu Griol, and Alejandro Martínez, “Resolving light handedness with an on-chip silicon microdisk,” *ACS Photonics* **1**, 762–767 (2014).
- [13] Immo Söllner, Sahand Mahmoodian, Sofie Lindskov Hansen, Leonardo Midolo, Alisa Javadi, Gabija Kiršanskė, Tommaso Pregnolato, Haitham El-Ella, Eun Hye Lee, Jin Dong Song, Søren Stobbe, and Peter Lodahl, “Deterministic photon-emitter coupling in chiral photonic circuits,” *Nature Nanotechnology* **10**, 775 (2015).
- [14] Peter Lodahl, Sahand Mahmoodian, Sren Stobbe, Arno Rauschenbeutel, Philipp Schneeweiss, Jürgen Volz, Hannes Pichler, and Peter Zoller, “Chiral quantum optics,” *Nature* **541**, 473 (2017).
- [15] Ben Lang, Ruth Oulton, and Daryl M Beggs, “Optimised photonic crystal waveguide for chiral light?matter interactions,” *Journal of Optics* **19**, 045001 (2017).
- [16] R.J. Coles, D.M. Price, J.E. Dixon, B. Royall, E. Clarke, P. Kok, M.S. Skolnick, A.M. Fox, and M.N. Makhonin, “Chirality of nanophotonic waveguide with embedded quantum emitter for unidirectional spin transfer,” *Nature Communications* **7**, 11183 EP – (2016).
- [17] B le Ferber, N Rotenberg, and L Kuipers, “Nanophotonic control of circular dipole emission,” *Nature Communications* **6**, 6695 (2015).
- [18] K. Y. Bliokh, F. J. Rodríguez-Fortuño, F. Nori, and

- A. V. Zayats, “Spin-orbit interactions of light,” *Nature Photonics* **9**, 796 (2015).
- [19] Sahand Mahmoodian, Peter Lodahl, and Anders S. Sørensen, “Quantum networks with chiral-light-matter interaction in waveguides,” *Phys. Rev. Lett.* **117**, 240501 (2016).
- [20] A. B. Young, A. C. T. Thijssen, D. M. Beggs, P. Androvitsaneas, L. Kuipers, J. G. Rarity, S. Hughes, and R. Oulton, “Polarization engineering in photonic crystal waveguides for spin-photon entanglers,” *Phys. Rev. Lett.* **115**, 153901 (2015).
- [21] R. J. Coles, D. M. Price, B. Royall, E. Clarke, M. S. Skolnick, A. M. Fox, and M. N. Makhonin, “Path-dependent initialization of a single quantum dot exciton spin in a nanophotonic waveguide,” *Phys. Rev. B* **95**, 121401 (2017).
- [22] Antoine Reigue, Jake Iles-Smith, Fabian Lux, Léonard Monniello, Mathieu Bernard, Florent Margaillan, Aristide Lemaitre, Anthony Martinez, Dara P. S. McCutcheon, Jesper Mørk, Richard Hostein, and Valia Voliotis, “Probing electron-phonon interaction through two-photon interference in resonantly driven semiconductor quantum dots,” *Phys. Rev. Lett.* **118**, 233602 (2017).
- [23] Andrei Faraon, Ilya Fushman, Dirk Englund, Nick Stoltz, Pierre Petroff, and Jelena Vučković, “Dipole induced transparency in waveguide coupled photonic crystal cavities,” *Opt. Express* **16**, 12154–12162 (2008).
- [24] I. J. Luxmoore, N. A. Wasley, A. J. Ramsay, A. C. T. Thijssen, R. Oulton, M. Hugues, S. Kasture, V. G. Achanta, A. M. Fox, and M. S. Skolnick, “Interfacing spins in an InGaAs quantum dot to a semiconductor waveguide circuit using emitted photons,” *Phys. Rev. Lett.* **110**, 037402 (2013).
- [25] Maxim N. Makhonin, James E. Dixon, Rikki J. Coles, Ben Royall, Isaac J. Luxmoore, Edmund Clarke, Maxime Hugues, Maurice S. Skolnick, and A. Mark Fox, “Waveguide coupled resonance fluorescence from on-chip quantum emitter,” *Nano Letters* **14**, 6997–7002 (2014).
- [26] I. J. Luxmoore, N. A. Wasley, A. J. Ramsay, A. C. T. Thijssen, R. Oulton, M. Hugues, A. M. Fox, and M. S. Skolnick, “Optical control of the emission direction of a quantum dot,” *Applied Physics Letters* **103**, 241102 (2013).
- [27] H. S. Nguyen, G. Sallen, C. Voisin, Ph. Roussignol, C. Diederichs, and G. Cassabois, “Optically gated resonant emission of single quantum dots,” *Phys. Rev. Lett.* **108**, 057401 (2012).
- [28] M. J. Collett and C. W. Gardiner, “Squeezing of intracavity and traveling-wave light fields produced in parametric amplification,” *Phys. Rev. A* **30**, 1386–1391 (1984).
- [29] Sahand Mahmoodian, Kasper Prindal-Nielsen, Immo Söllner, Søren Stobbe, and Peter Lodahl, “Engineering chiral light-matter interaction in photonic crystal waveguides with slow light,” *Opt. Mater. Express* **7**, 43–51 (2017).
- [30] Clément Sayrin, Christian Junge, Rudolf Mitsch, Bernhard Albrecht, Danny O’Shea, Philipp Schneeweiss, Jürgen Volz, and Arno Rauschenbeutel, “Nanophotonic optical isolator controlled by the internal state of cold atoms,” *Phys. Rev. X* **5**, 041036 (2015).
- [31] Clément Sayrin, Christian Junge, Rudolf Mitsch, Bernhard Albrecht, Danny O’Shea, Philipp Schneeweiss, Jürgen Volz, and Arno Rauschenbeutel, “Nanophotonic optical isolator controlled by the internal state of cold atoms,” *Phys. Rev. X* **5**, 041036 (2015).